Journal of Applied Fluid Mechanics, Vol. 10, No. 6, pp. 1689-1697, 2017.
Available online at www.jafmonline.net, ISSN 1735-3572, EISSN 1735-3645.
DOI: 10.29252/jafm.10.06.26959

Aerodynamics of Flapping Wings for Vertical Takeoff

G. C. Vishnu Kumar † and D. A. Shah

Hindustan University, Chennai, India

†*Corresponding Author Email: rs.vkgc0914@hindustanuniv.ac.in*

(Received July 20, 2016; accepted July 16, 2017)

ABSTRACT

The present study is based on analysing a flapping based locomotion in vertical direction which is inspired from jelly fish in vertical locomotion. A numerical investigation is performed to analyse the aerodynamic performance in terms of two dimensional flat plates under flapping conditions with the fluid at rest. The model considered is an umbrella structure prototype which has vertical plates placed at certain intermittent distance from each other with their leading edges hinged. The dynamic effect of 2D plates are analysed by varying the chord length of flapper for a range of amplitude and frequency to study the interference effects of flappers in close proximity. It is found that a suitable chord length and intermittent distance is required for improving the aerodynamic characteristics. It is envisaged that the results obtained in this study will lead to better understanding of the dynamics of flapping based locomotion which are useful for developing hovering kinematics in surveillance and reconnaissance.

Keywords: Flapping; Flat plates; Numerical simulation; Vortex structure.

NOMENCLATURE

A	maximal tip displacement	f	frequency in Hertz
c	chord length	p	pressure
C_D	drag Coefficient	Re	Reynolds number
C_L	lift coefficient	St	Strouhal number
Cy	force coefficient in the y direction	u	velocity component in x direction
ΔC_D	drag Coefficient	v	velocity component in y direction
ΔC_L	lift coefficient		
d	inter-distance between flappers	θ	flapping amplitude in degrees
dt	time step	ρ	density

1. INTRODUCTION

Ornithopters imitate the flapping flight of flying species from birds to insects. It achieves stability by its symmetrical pair of wings. Flapping wings offer potential advantages over fixed wings in its maneuverability and energy savings at low speed and at mini scale level. The observations of birds and insects flight reveal that they have a unique pattern of flappers in pair which is suitable for their body muscles. Also some of the birds can use their wings for flapping as well as hovering capability. The flapping wings has combined function of lift and thrust which reduces the drag inducing structures. Hence high degree of efficiency for lift and hovering ability is needed. It should also be lightweight with easy drive mechanisms. To have the vertical flapping wing kinematics, optimal aerodynamic performance needs to be analysed. Wan *et al.* (2012) analysed the interaction of hovering hinged plate with passive deflection in horizontal direction by varying the stroke amplitude. The increases in the stroke amplitude to chord length ratio increases the lift coefficient of the flapper. The effect of Reynolds number on lift and thrust forces of flapping a corrugated airfoil is numerically investigated by Tang *et al.* (2008). The flow physics indicates the enhancement of stall phenomenon and wake capturing with the increase in Reynolds number. Also the lift coefficient increases as the stroke plane angle changes. Hence stroke amplitude is a major factor which significantly increases the characteristics of aerodynamic forces. Jones *et al.* (2005) analysed on a pair of flapping wings placed at the trailing

edge of fixed wing. The symmetric nature of the flapping-wing provides mechanical and aerodynamic balancing, and improved the aerodynamic performance. The flapping-wing pair provided with camber improves the performance at lower frequencies while at higher frequencies performance degrades as compared to flat plate flapping pair wings. Also the angle of attack to free stream flow with double flappers in close proximity is also a major factor for increasing the aerodynamic efficiency. Sun and Xiong (2005) computed the longitudinal stability of hovering bumble bee. During its motion it is dynamically stable and the disturbances gets damped with adjustment to its wing kinematics, and returns to the equilibrium automatically. Hence a continuous adjustment to its wing kinematics is necessary in order to keep to the reference flight, and the disturbed motion predicted by the model would be altered at an early stage. Zdunich *et al.* (2007) developed a flapping-wing model, which uses clap-fling phenomenon to study the effects on stability during hovering. The two sets of wings help in eliminating the side to side flapping forces. Ristroph and Childress (2014) developed a model that opens and closes four wings, resembling the motion of swimming jellyfish. The model reveals that there is a need of further analysis for the length of flapper, its intermittent distance and frequency for achieving maximum efficiency. Weis-Fogh (1973) analysed on a pair of wings with clap and fling mechanism sequentially to enhance the aerodynamic performance with flapping at close proximity. Also a study by Shy *et al.* (2008) have shown that under flapping conditions of certain value of mean angle of attack, the results of two dimensional models agree well with three dimensional models with the plate thickness 1% of its chord length. Mahboubi *et al.* (2016) analysed on the lift of flexible flapper increases beyond 8 Hz than the rigid flapper. Hence rigid flappers can perform better under 10Hz beyond which flexibility is required for higher frequencies. The flapping motion initiated in the present model is similar to the movement of jellyfish in water medium. The plates are hinged at its leading edge and are allowed to flap along the hinge location. Consequently, lift is in the positive y direction, while drag is in the direction opposite of the time varying velocity.

The present paper is organized as follows. The flapping kinematics and its behaviour is described in section 2. In section 3, the problem description is discussed. The computational method is discussed in section 4 and kinematics in section 5. The validation of the code, grid convergence and cycle convergence are presented in section 6. The results of instant lift/drag force variations of flappers in close proximity is analysed with vorticity contours in section 7. Finally, the conclusions are summarized with key points.

2. THE CONCEPT

The conceptual sketch consists of a jellyfish – umbrella hybrid prototype which uses a motor with linkages to produce up and down sliding motion connected to a central stick which houses the ribs as shown in Fig. 1. Each rib is connected to its individual flappers hinged at its one end around the central hub. As the motor rotates the linkages, the rotary motion is transferred to the flappers by pulling it in and pushing it out. The central ring supports the flapping wing. Also critical adjustments are needed for higher flapping frequency. To understand the flapping kinematics, a two dimensional model of flappers at certain intermittent distance is initially analysed. The diameter of the flapping wing prototype will be used as intermittent distance, d in the 2-dimensional model.

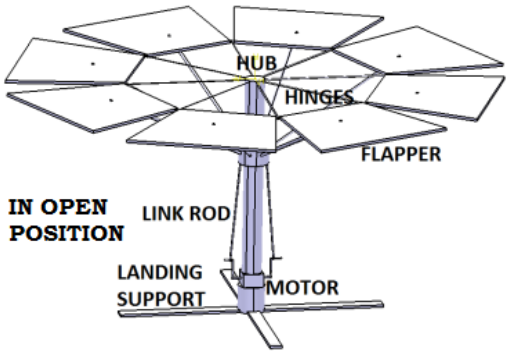

(a)

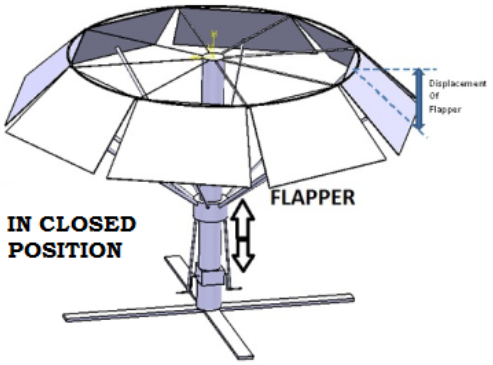

(b)

Fig. 1. Flapper in (a) open position (b) closed position.

3. PROBLEM DEFINITION

The present approach is to develop a model consisting of two dimensional vertical flapping plates of chord length, c placed at a distance, d with respect to each other as shown in Fig. 2a. As the plate is hinged on its leading edge the horizontal displacement is constrained. Based on Wang *et al.* (2004) the 3D model can be simplified to 2D model as the present study is axisymmetric. The length of the flappers are varied from 5cm to 20cm in the increment of 5cm. Also flapping

amplitude and frequency are varied to observe the effects on average lift and drag for vertical liftoff efficiency. The flapping amplitude is varied from 30° - 60° in the increment of 15° while the frequency is varied from 5-15 Hz in the increment of 5 Hz to observe the overall effect in broader range for each parameter by analysing the average lift and drag coefficients. As the model requires analysis for various flapping frequency and amplitude, a total of 30 cases are discussed in the following sections. For initial consideration the intermittent distance is fixed at 5cm and length of the flapper is increased to get the required d/c ratios as shown in Table 1.

Table 1 Parametric study of flapping wings in the present study

d/c	Amplitude, θ (degrees)	Frequency, *f* (Hz)
0.25	30° - 60°	5-15
0.3		
0.5		
0.75		
1.0		

4. GOVERNING EQUATIONS

Because of the low Reynolds number flow characteristics, the fluid flow equation for the 2D, laminar, incompressible flow with constant flow properties employed as governing equations are denoted as

$$\frac{\partial u}{\partial x} + \frac{\partial v}{\partial y} = 0 \tag{1}$$

$$\frac{\partial u}{\partial t} + \frac{\partial (uu)}{\partial x} + \frac{\partial (uv)}{\partial y} = -\frac{\partial_P}{\partial x} + \frac{1}{Re}\left(\frac{\partial^2 u}{\partial x^2} + \frac{\partial^2 v}{\partial y^2}\right) \tag{2}$$

$$\frac{\partial v}{\partial t} + \frac{\partial (uv)}{\partial x} + \frac{\partial (vv)}{\partial y} = -\frac{\partial_P}{\partial y} + \frac{1}{Re}\left(\frac{\partial^2 v}{\partial x^2} + \frac{\partial^2 v}{\partial y^2}\right) \tag{3}$$

The Reynolds number for the present model is in the order of 10^4 based on the previous experimental studies of Ristroph (2014). Hence flappers are flapping at relatively less frequency with viscous laminar model chosen for the present study. The PISO (Pressure-Implicit with Splitting of Operators) coupling scheme developed by ISSA (1986) is used along with transient conditions with first order discretization scheme and first order implicit formulation with convergence criteria of 1x e^{-4} for residuals of each time step. The following steps are followed during the algorithm which solves the Navier stokes equations. It splits the solution process into a series of predictor and corrector steps with transient flow computational efficiency.

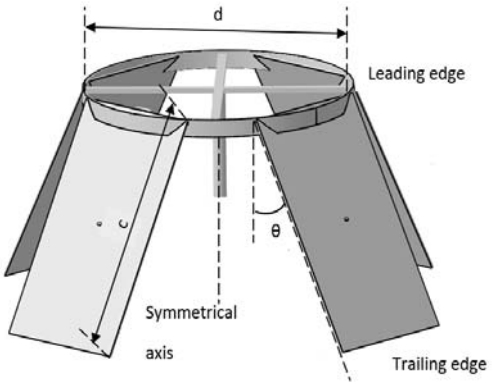

(a)

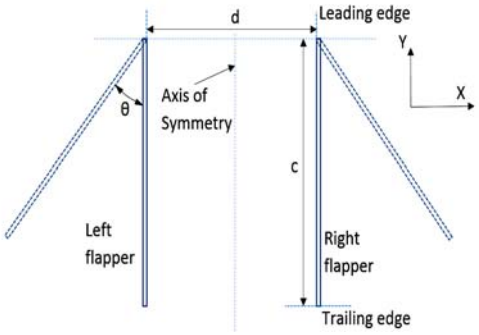

(b)

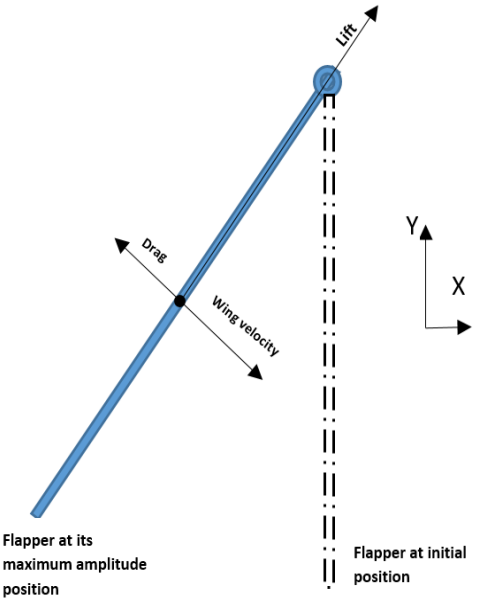

(c)

Fig. 2. (a) Sketch illustrating the 3D view of flappers (b) 2D view of flapper with chord length, c hinged at its leading edge with intermittent distance, d (c) aerodynamic force components of flapper.

Step 1. Initial guess of p^*, u^*, v^*, φ^*

Step 2. Solving discretized momentum equations to get u^*, v^*

$$a_{i,j}u^*_{i,j} = \sum a_{nb}u^*_{nb} + (p^*_{i-1,j} - p^*_{i,j})A_{i,j} + b_{i,j}$$
$$a_{i,j}v^*_{i,j} = \sum a_{nb}v^*_{nb} + (p^*_{i,j-1} - p^*_{i,j})A_{i,j} + b_{i,j}$$

Step 3. Solving pressure correction equation to get p'

$$a_{i,j}p'_{i,j} = a_{i-1,j}p'_{i-1,j} + a_{i+1,j}p'_{i+1,j}$$
$$+a_{i,j-1}p'_{i,j-1} + a_{i,j+1}p'_{i,j+1} + b_{i,j}$$

Step 4. Correcting pressure and velocities to get p *, u*, v*, p '

$$p_{i,j} = p^*_{i,j} + p'_{i-1,j}$$
$$u_{i,j} = u^*_{i,j} + d_{i,j}(p_{i-1,j} - p'_{i,j})$$
$$v_{i,j} = v^*_{i,j} + d_{i,j}(p'_{i,j-1} - p'_{i,j})$$

Step 5. Solving second pressure equation:

$$a_{i,j}p''_{i,j} = a_{i-1,j}p''_{i-1,j} + a_{i+1,j}p''_{i+1,j}$$
$$+a_{i,j-1}p''_{i,j-1} + a_{i,j+1}p''_{i,j+1} + b''_{i,j}$$

Step 6. Correcting pressure and velocities terms:

$$p^{***}_{i,j} = p^*_{i,j} + p'_{i,j} + p''_{i,j}$$

$$u^{***}_{i,j} = u^*_{i,j} + d_{i,j}(p'_{i-1,j} - p'_{i,j})$$
$$+\frac{\sum a_{nb}(u^{**}_{nb} - u^*_{nb})}{a_{i,j}} + d_{i,j}(p''_{i-1,j} - p''_{i,j})$$

$$v^{***}_{i,j} = v^*_{i,j} + d_{i,j}(p'_{i,j-1} - p'_{i,j})$$
$$+\frac{\sum a_{nb}(v^{**}_{nb} - v^*_{nb})}{a_{i,j}} + d_{i,j}(p''_{i,j-1} - p''_{i,j})$$

Step 7. Setting $p = p^{***}, u = u^{***}, v = v^{***}$ to get p, u, v, φ^*

Step 8. Solving discretized transport equations to get φ

$$a_{i,j}\varphi_{i,j} = a_{i-1,j}\varphi_{i-1,j} + a_{i+1,j}\varphi_{i+1,j}$$
$$+a_{i,j-1}\varphi_{i,j-1} + a_{i,j+1}\varphi_{i,j+1} + b_{i,j}$$

Step 9. Checking for convergence

If yes then solution is achieved

If no then repeating the process again from step 1. $p^* = p, u^* = u, v^* = v, \varphi^* = \varphi$

Also mesh update methods such as smoothing and remeshing option is provided for dynamic mesh simulations.

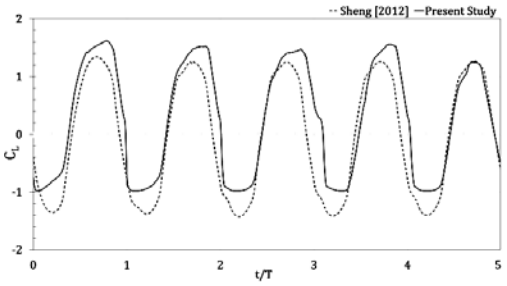

(a)

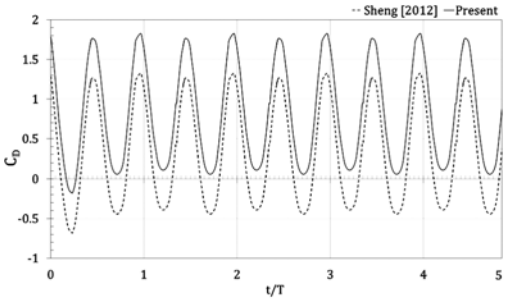

(b)

Fig. 3. (a) Lift coefficient and (b) Drag coefficient for the present study and equivalent instants in Sheng (2012) at Reynolds number = 1000.

5. FLAPPING WING KINEMATICS

The flapping kinematics of the present study involving flat plate hinged at its leading edge is given by the equation

$$\theta(t) = \theta_0 \sin\left(2\pi f t\right)$$

The flapping wing starts from its vertical alignment position in still air and flaps on both its sides towards outer region from its vertical position. In C program, a user defined function (UDF) is interpreted in FLUENT for flapping simulation of the plates. In the mesh motion tab the leading edge of the flappers are hinged by providing its c.g. location of the flappers in xy plane.

The flapping cycle is initiated and at regular intervals the tet elements are continuously improved by remeshing technique.

6. COMPUTATIONAL METHOD

The code used in the present study is for low Reynolds number flow field situations. Hence a single grid solver is chosen as the mesh will be deformed with change in its intermittent distance. The outer boundary is defined as pressure outlet.

The boundary conditions for the meshed domain are shown in Fig. 4a. The outer domain is meshed coarse as shown in Fig. 4b, while an intermediate domain is modelled for creating fine mesh as shown in Fig. 5a. The flappers is provided with wall and no slip boundary conditions as shown in Fig. 5b.

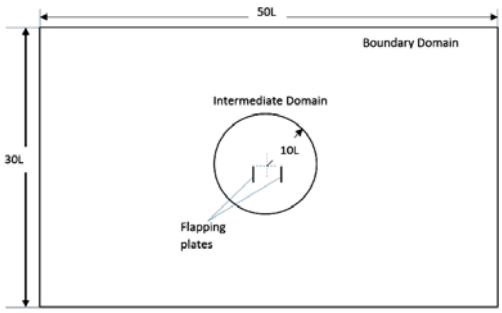

(a)

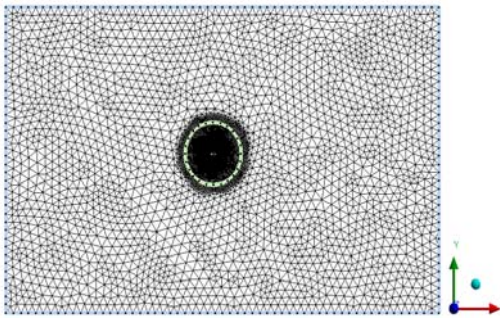

(b)

Fig. 4. (a) Boundary domain (b) Outer domain.

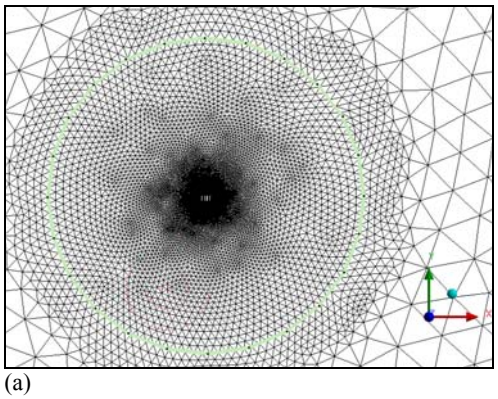

(a)

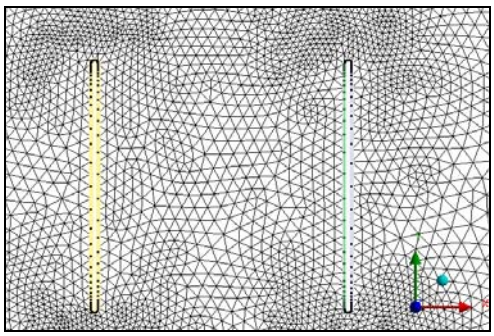

(b)

Fig. 5. Meshed Model (a) Intermedate domain (b) Flappers.

6.1 Grid and Cycle Independent Study

To check the spatial accuracy of the present case, grid independence study is carried out for d/c = 1, frequency =10Hz, amplitude =30°. To examine the grid dependency on the size of computational domain, rectangular computational domain with a size of 50L x 30L are meshed initially where the first grid is located at 10L from the wing surface. The mesh size is varied from 3×10^4, 4×10^4 and 6×10^4 elements in the intermediate domain. The timestep is increased and convergence is checked for every iteration. The solver numerically computes the Navier-Stokes equations with its velocity and pressure components updated at discretized grid locations for each time step. Hence integrating the viscous and pressure terms over the profile provides the aerodynamic force at each time step. The remeshing method will compute the mesh layer at each time step to calculate the elastic forces.

The C_L and C_d are in reasonable agreement for different grids, which indicates that the simulation results are independent on the grid numbers for the cases selected. From Fig. 6(a) and 6(b) it can be observed that intermediate mesh of $4x10^4$ elements is providing grid independent characteristics. The cycle averaged aerodynamic coefficients to be mesh independent as shown in Figs. 6(a) and 6(b). The average value of aerodynamic coefficients are presented in Table 2.

Table 2Grid independent study

d/c	Aerodynamic force coefficient	Grid System		
		1	2	3
1.0	ΔC_L	0.1	0.07	0.08
	ΔC_D	0.04	0.19	0.21

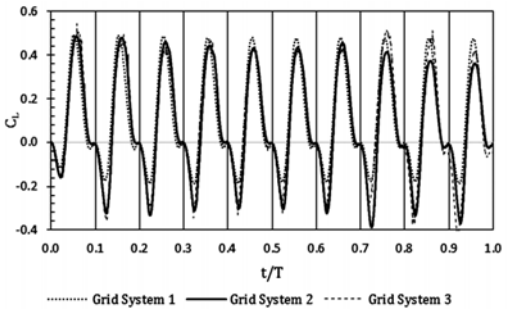

(a)

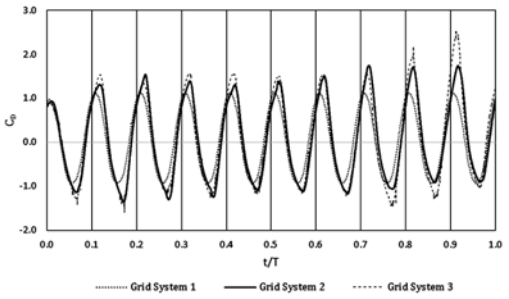

(b)

Fig. 6. Convergence study of grid: (a) lift Coefficient, and (b) drag coefficient at f = 10 Hz and θ_0= 30°.

The flappers are assumed as wall, and is modeled as

thin membrane, while the outer domain is considered to be pressure outlet where the airflow is allowed to pass through. The domain is constructed in ANSYS Design modeler while the computational domain in mesh modeler is inbuilt.

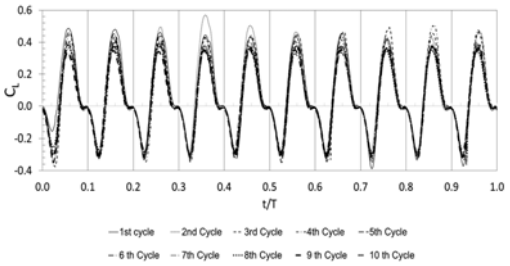

(a)

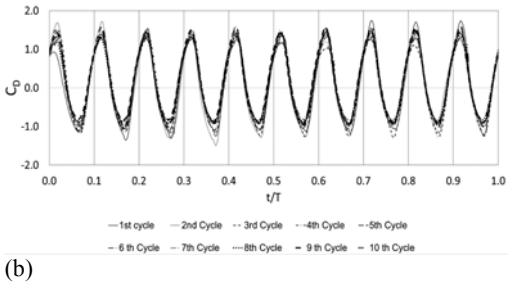

(b)

Fig. 7. Convergence study of cycle: (a) lift Coefficient, and (b) drag coefficient at f = 10 Hz and θ_0= 30°.

6.2 Validation

The present study is validated with a preliminary run on flapping plate of Sheng *et al.* (2012) where the plates are hinged at its leading edge and for flow conditions of Re=1000, *f*=5 Hz, St=0.4, A=0.8. The numerical results of lift and drag coefficients are presented in Fig. 3 for validation. There exists a similarity between the two studies as the flapper is undergoing similar boundary conditions.

7. RESULTS AND DISCUSSION

In order to investigate the effect of varying d/c ratio, the intermittent distance is kept at 5 cm while the length of flapper is increased to get the required d/c ratio. Amplitude and frequency are varied to find the effective $\Delta C_L/\Delta C_D$ for vertical liftoff efficiency. The plates are restrained for flapping with their amplitude varied from the initial position along the axis of symmetry. The maximum $\Delta C_L/\Delta C_D$ ratio is observed for d/c = 0.5 for the amplitude 30° of flappers from the Fig. 8a.

As the length of flapper increases, decreasing the d/c ratio below 0.5 makes the flapper producing weaker lift characteristics as evident from the Fig. 8 and in order to get high lift in this range, lower frequency is required to reduce high pressure region developed at the trailing edge as shown in Fig. 8b. Also as amplitude increases to 60°, the $\Delta C_L/\Delta C_D$ is reaching comparatively high values. This is due to the plate length in backward stroke produces high flow of air to stack in the middle region and it gets compressed at the time of stroke reversal. The average $\Delta C_L/\Delta C_D$ for every d/c ratio indicates that lower frequency requires lower amplitude with higher d/c ratio. Hence large flappers at high frequency produces less lift as amplitude is decreased from the Fig. 8c.

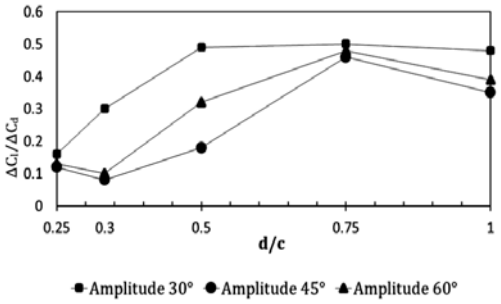

(a)

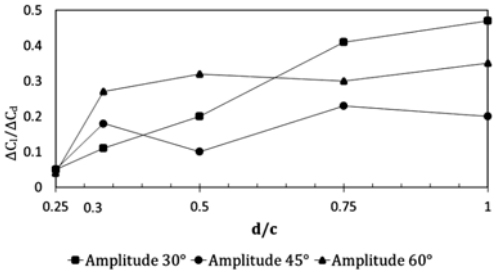

(b)

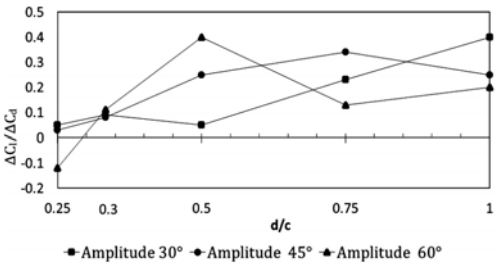

(c)

Fig. 8. Variation of $\Delta C_L/\Delta C_D$ with d/c ratio (a) frequency 5 Hz, (b) frequency 10 Hz, (c) frequency 15 Hz.

For d/c = 1 maximum positive $\Delta C_L/\Delta C_D$ is achieved when the amplitude reaches 30°. It is due to the fact that the intermittent distance is high and uniform mixing of airflow is achieved at shorter time interval. The vortex pair developed at the trailing edge provides additional lift enhancement to the flapper at the end of the cycle. Also when the flappers are at d/c = 0.25, amplitude 30° seems to be providing efficient lift. The interference effect provides that the force coefficients vary slightly for lower d/c. A moderate amplitude of 30° can be chosen as it provides higher efficiency characteristics at d/c =0.5 with flappers length as 10cm. According to Defense Advanced Research Projects Agency (DARPA) regulations, micro aerial vehicle needs to be within the size limit of 15cm in all its sides. Hence d/c = 0.3 (c=15 cm flapper) is analysed as an additional case to determine the

efficiency of the enclosed region. For d/c = 0.3, the value of C_L/C_D is not varying relatively for increase in amplitude and frequency. It is evident that there is a tradeoff between the effects of lift sacrifice and drag reduction which influences the d/c ratio at these regimes. If there is relatively less frequency then amplitude comes into effect of compensating the lift distribution with the intermittent distance providing a smooth airflow to pass through the centre. The flappers at maximum position induces the trailing edge vortices which is stronger than leading edge vortices.

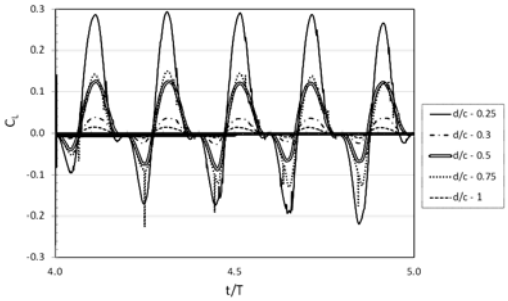

Fig. 9. Variation of C_L at maximum C_L / C_D for various d/c ratio.

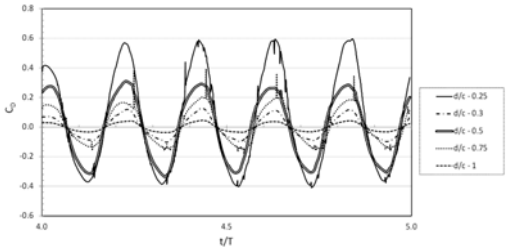

Fig. 10. Variation of C_D at maximum C_L / C_D for various d/c ratio.

The forces are presented in the form of non-dimensional force coefficients as C_L and C_D in Figs. 9 and 10 respectively for the peak case of $\Delta C_L/\Delta C_D$ at every d/c ratio from Fig. 8(a)-(c). From Fig. 9 we can observe that maximum peak are synchronous with each other, while the amplitude of the profile varies according to the chord length of flapper. Though the average lift is higher for d/c = 0.25 comparing to other cases, the average drag is also relatively higher which reduces the value of $\Delta C_L/\Delta C_D$. It can be observed from Fig. 10 that fluctuations of $\Delta C_L/\Delta C_D$ decreases by increasing the d/c ratio. The amplitude of the flapper is almost independent for lower d/c while significant value of $\Delta C_L/\Delta C_D$ can be seen at higher d/c values. Also at higher amplitudes of 60° at d/c = 1 the variation of C_L/C_D has significant effect and hence the length of flapper is significant to get the aerodynamic efficiency. For small flappers, lower amplitude and lower frequency is providing efficiency. Also for large flappers, lower amplitude is required as can be seen from the highest $\Delta C_L/\Delta C_D$ peak points. The vorticity vector representation of flappers for lowest and highest values of $\Delta C_L/\Delta C_D$ at frequency of 10 Hz for variations in d/c ratio is shown in Fig. 11 and 12 respectively.

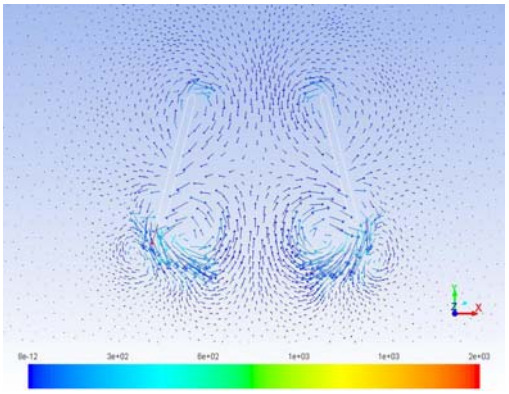

(a) d/c = 1, Amplitude= 30°

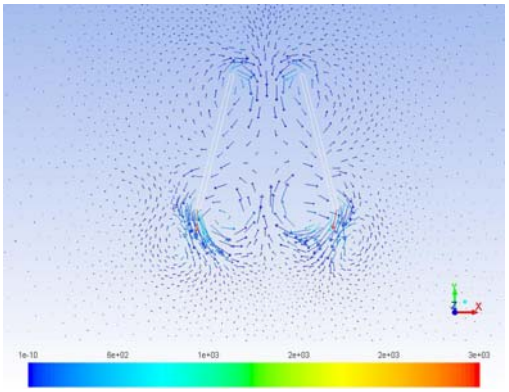

(b) d/c = 0.5, Amplitude = 30°

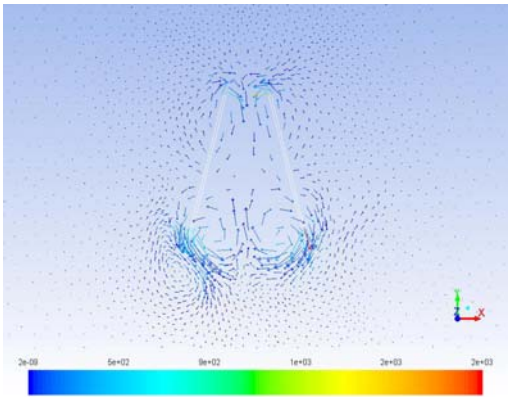

(c) d/c = 0.3, Amplitude = 30°

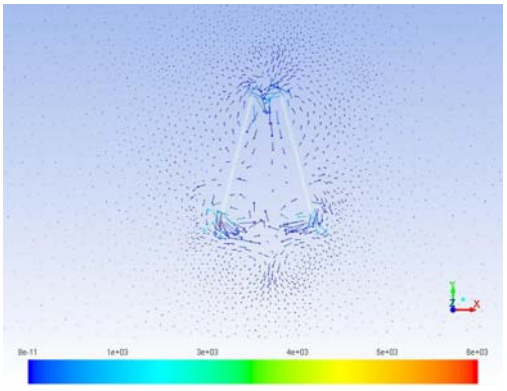

(d) d/c = 0.25, Amplitude = 30°

Fig. 11. Vorticity vector representation of flappers for highest values of $\Delta C_L/\Delta C_D$.

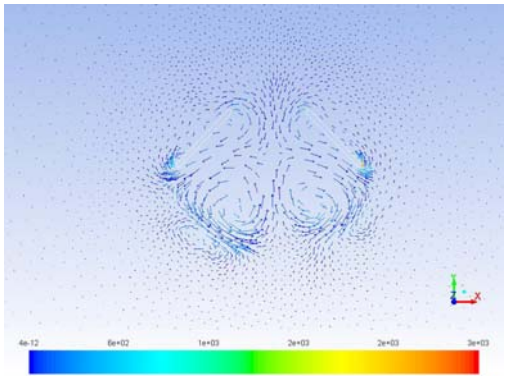

(a) d/c = 1, Amplitude = 60°

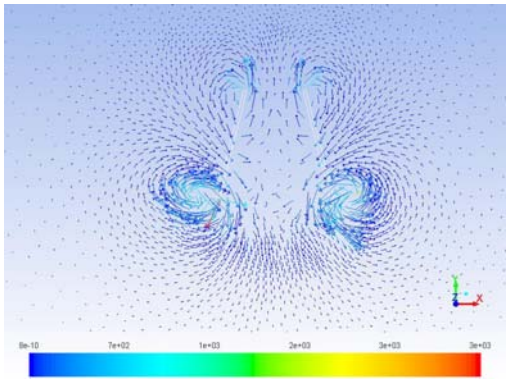

(b) d/c = 0.5, Amplitude = 30°

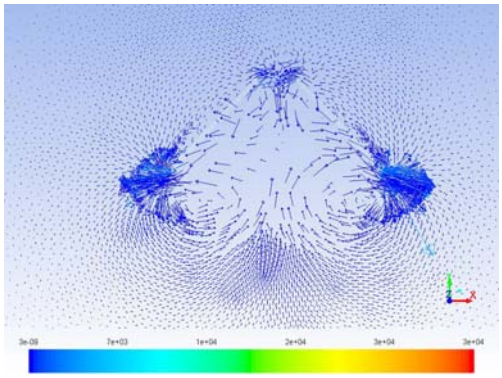

(c) d/c = 0.3, Amplitude = 60°

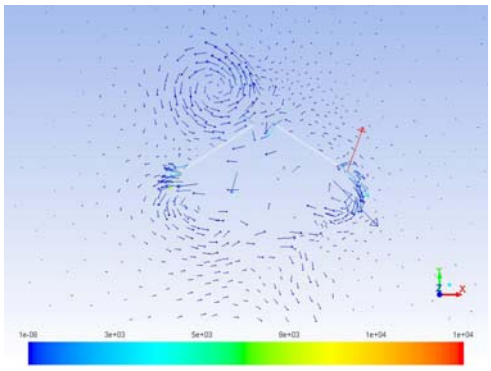

(d) d/c = 0.25, Amplitude = 60°

Fig. 12. Vorticity vector representation of flappers for lowest values of $\Delta C_L/\Delta C_D$.

From Fig. 11 there is uniform pattern on vorticity contours on both sides of the flappers as the flappers considered is symmetrical about y axis. The primary vortex induced at the flapping plate's trailing edge is moving away as the flapper starts its cycle towards the maximum position. On the other hand, the initial pressure developed on the inner layer of the plate shifts towards the trailing edge, as the plates comes closer in flapping motion. At the same time, outer surface of the plates gets high pressure distribution compared to the inner surface. The low pressure region generated in the inner layer of the flappers develop into a fully developed region which moves towards the trailing edge. For the case of d/c = 0.75, contributions from both the flappers requires significant intermittent distance. But when the plates flap continuously, air is accelerated towards the trailing edge which reduces the high pressure stagnation area. Hence high d/c ratio is required which ensures the wake recapture by the influence of primary and secondary vortices. After the flapper reaches the maximum position, it will be completing its half cycle. When the flappers are reaching towards the initial vertical position for full cycle to complete, the pressure region changes from outer surface to inner surface with high pressure developed underneath the flapper's surface. The phenomenon of change of pressure region continues from the inner to outer surface of the flappers over the entire cycle. From Fig. 12(d), the flappers are at a distance far away from each other which even at high flapping rate effective velocity is not feasible as flow at the end of the down stroke produces negative lift. By increasing the amplitude for this case provides no significant change in increasing the lift characteristics as relative mixing of airflow at the region in between the flappers is not guaranteed. For d/c = 0.5 mixing of airflow can be seen at an early stage of the cycle and resultant velocity from the flappers is uniform. At the end of one complete cycle, flow is converged with increase in its velocity compared to the previous case. For d/c = 0.5, a fully developed vortex towards trailing edge is observed. At the end of the completed cycle, the trailing edge vortex detaches which is very weak to grow at less amplitude. For d/c = 1, the induced velocity field developed by the counter rotating vortices is detaching from the inner surface of the flappers at its trailing edge. Though the intermittent distance facilitates the compression of airflow as a duct, the flapper length influences the increase in drag characteristics by the suppression of leading edge vortices.

The present results are validated by comparing them with similar results of past studies, where a direct comparison in terms of geometric and kinematic parameters is not feasible. Wan *et al.* (2012) analysed for one link plate where the plates are allowed to move horizontally with variable flapping stroke amplitude to chord ratio at Reynolds number of 200. The translation and rotation of the flapper are in phase with each other. As stroke-to-chord ratio increases from 1 to 3, the lift-to – drag ratio rises quickly after which the change is very gradual with the inclination angle is limited at 45°. It indicates that increasing the stroke – chord ratio beyond certain limit is not providing significant

improvement for the flappers. The stroke amplitude to chord length of the flapper is varied from A_x/c = 1 to 6 which increased the average of C_L/C_D from -0.4 to 0.6. In the present study the optimum flappers corresponding to frequency of 10 Hz has variations from 0.25 to 1 which increased the $\Delta C_L/\Delta C_D$ from 0.05 to 0.48. Hence it can be compared that the leading edge hinged flappers provides positive lift and it is affected by the intermittent distance to chord length of the flapper. Also a similar study with elliptic profile is analysed by Sebastian *et al.* (2013) where a parametric study on aerodynamic performance of flapping wings at Reynolds number of 1400 shows that the effect of mean angle of attack increases lift. Recently Leif Ristroph (2014) worked on a flapping model, to get the necessary length of flapper to be around 8~11 cm and flapping frequency of 10 Hz to get maximum lift. Thus we see that the flapper chord length and its intermittent distance plays a major role in the development of lift characteristics to get uniform flow from the flappers.

8. CONCLUSION

The mean lift to drag coefficient is analysed to get the optimised length and intermittent distance of the flappers. From the present study we can acquire that the small flappers flapping at high frequency and large flappers at low frequency generates weaker lift characteristics. The positive lift of large flappers at low frequency is comparatively less to other models considered. The flappers with chord length of 10cm and intermittent distance of 5cm is providing the significant lift contribution. The variation in the value of average lift to drag coefficients of large flappers suggests that changing the flapping frequency and amplitude is not having significant improvement concluding that the flappers should not be too close to each other. Also at higher amplitudes, flappers in close proximity will not provide the interference effect to improve the lift characteristics. Flow visualization studies of swimming jellyfish have shown that the inward motion of flapper generates higher flow velocity by Dabiri (2005) and Peng (2012). Further analysis on the flapping mode in terms of outward, inward and symmetrical can be analysed in future work to get the efficient aerodynamic characteristics.

REFERENCES

Dabiri, J. O., S. P. Colin, J. H. Costello and M. Gharib (2005). Flow Patterns Generated by Oblate Medusan Jellyfish: Field Measurements and Laboratory Analyses. *Journal of Experimental Biology* 208, 1257-1269.

Issa, R. I. (1986). Solution of Implicitly Discretized Fluid Flow Equations by Operator Splitting. *Journal of Computational Physics* 62, 40-65.

Jones, K. D., C. J. Bradshaw, J. Papadopoulos and M. F. Platzer (2005). Bio-inspired design of flapping-wing micro aerial vehicles. *Aeronautical Journal* 109(2005), 385-393.

Leif, R. and S. Childress (2014). Stable hovering of a jelly fish like flying machine. *Journal of Royal Society Interface* 11, 20130992.

Mahboubi Doust, A., A. Ramiar and M. Dardel (2016). Simultaneous investigation of flexibility and plasma actuation effects on the aerodynamic characteristics of an oscillating airfoil. *Journal of Applied Fluid Mechanics* 9(5), 2489-2501.

Peng, J. and S. Alben (2012). Effects of shape and stroke parameters on the propulsion performance of an axisymmetric swimmer. *Bio inspiration Biomimetics* 7, 016012.

Sebastian, l. and O. Lopez (2013). Parametric study of low Reynolds number flapping wing aerodynamics. *AIAA Journal* 54, 42-51.

Sheng, J. X., A. Yasi, D. Kolomensky, E. Kanso, M. Nitsche and K. Schneider (2012). Simulating vortex wakes of flapping plates, *Natural Locomotion in Fluids and on surfaces* 155, 255-262.

Sun, M. and Y. Xiong (2005). Dynamic flight stability of a hovering bumblebee. *Journal of Experimental Biology* 208, 447–459.

Wan, H., H. Dong and G. P. Huang (2012). Hovering Hinge-connected flapping plate with passive deflection. *AIAA Journal* 50, 2020–2027.

Wang, Z., J. Birch and M. Dickinson (2004). Unsteady forces and flows in low Reynolds number hovering: two-dimensional computations vs robotic wing experiments. *Journal of Experimental Biology* 207, 449-460.

Weis Fogh, T. (1973). Quick estimates of flight fitness in hovering animals, including novel mechanisms for lift production. *Journal of Experimental Biology* 5, 169–230.

Zdunich, P., D. Bilyk, M. MacMaster, D. Loewen, J. DeLaurier, R. Kornbluh, T. Low, S. Stanford and D. Holeman (2007). *Development and testing of the* Mentor flapping-wing micro air vehicle. *Journal of Aircraft* 44, 1701–1711.